



PCCP

Influence of humidity and iron (III) on photodegradation of atmospheric secondary organic aerosol particles

Journal:	<i>Physical Chemistry Chemical Physics</i>
Manuscript ID	CP-ART-06-2018-003981.R1
Article Type:	Paper
Date Submitted by the Author:	18-Oct-2018
Complete List of Authors:	Arroyo, Pablo; Paul Scherrer Institut; University of Bern, Department of Chemistry and Biochemistry Malecha, Kurtis; University of California at Irvine, Department of Chemistry Ammann, Markus; Paul Scherrer Institut, Nizkorodov, Sergey; University of California at Irvine, Department of Chemistry

SCHOLARONE™
Manuscripts

1 Influence of humidity and iron (III) on
2 photodegradation of atmospheric secondary
3 organic aerosol particles
4

5 *Pablo Corral Arroyo^{1,2}, Kurtis T. Malecha³, Markus Ammann¹, Sergey A.*

6 *Nizkorodov^{3,*}*

7 1. Paul Scherrer Institute, Laboratory of Environmental Chemistry, 5232 Villigen PSI,

8 Switzerland.

9 2. Department of Chemistry and Biochemistry, University of Bern, 2012 Bern,

10 Switzerland.

11 3. Department of Chemistry, University of California, Irvine, California 92697, United

12 States

13 E-mail: nizkorod@uci.edu

14 ABSTRACT

15 The absorption of solar actinic radiation by atmospheric secondary organic aerosol (SOA) particles
16 drives condensed-phase photochemical processes, which lead to particle mass loss by the production
17 of CO, CO₂, hydrocarbons, and various oxygenated volatile organic compounds (OVOCs). We
18 examined the influence of relative humidity (RH) and Fe(III) content on the OVOC release and
19 subsequent mass loss from secondary organic aerosol material (SOM) during UV irradiation. The
20 samples were generated in a flow tube reactor from the oxidation of d-limonene by ozone. The SOM
21 was collected with a Micro Orifice Uniform Deposit Impactor (MOUDI) on CaF₂ windows. To
22 selected samples, a variable amount of FeCl₃ was added before irradiation. The resulting SOM

23 samples, with or without added FeCl_3 , were irradiated with a 305 nm light-emitting diode and the
24 release of several OVOCs, including acetic acid, acetone, formic acid and acetaldehyde, was
25 measured with a Proton Transfer Reaction Time-of-Flight Mass Spectrometer (PTR-ToF-MS). The
26 release of OVOCs from photodegradation of SOM at typical ambient mid-values of RH (30-70%) was
27 2-4 times higher than under dry conditions. The release of OVOCs was slightly enhanced in the
28 presence of low concentrations of iron (0.04 Fe molar ratio) but it was suppressed at higher
29 concentrations (0.50 Fe molar ratio) of iron indicating the existence of a complicated radical
30 chemistry driving the photodegradation of SOM. Our findings suggest that the presence of iron in
31 atmospheric aerosol particles will either increase or decrease release of OVOCs due to the
32 photodegradation of SOM depending on whether the relative iron concentration is low or high,
33 respectively. At atmospherically relevant RH conditions, the expected fractional mass loss induced by
34 these photochemical processes from limonene SOA particles would be between 2 and 4% of particle
35 mass per hour. Therefore, photodegradation is an important aging mechanism for this type of SOA.

36 INTRODUCTION

37 Organic compounds constitute a substantial fraction of atmospheric aerosol particles. They are present
38 at an overall mass concentration that is comparable to that of major inorganic species such as sulfates,
39 nitrates, sea salt and mineral dust components.¹ These organic compounds come from primary organic
40 aerosol (POA), which is emitted directly by various sources, or from secondary organic aerosol
41 (SOA), which is derived from reactions of volatile organic compounds (VOCs) with oxidants.¹ The
42 distinction between the primary and secondary particles blurs as particles are aged by physical
43 changes, such as gas-particle partitioning, particle coagulation or phase transitions within particles,
44 and chemical processes such as reactive uptake of gas-phase oxidants by the particles.² Recent studies
45 have shown that multiphase chemistry and photochemistry may significantly contribute to aging and
46 particle growth.²⁻⁴

47 Particle phase photochemistry contributes to aerosol aging by multiple mechanisms. Energy-transfer
48 or charge-transfer reactions driven by triplet states of organic compounds,⁵⁻⁷ photolysis of nitrate and
49 nitrite resulting in free radicals,⁸ photochemistry of iron carboxylate or free iron,⁹ and photolysis of
50 carbonyls^{10, 11} are some of the examples of these processes. The condensed-phase photochemical
51 reactions may not only change the SOA composition, but also change the volatility distribution of the
52 SOA compounds resulting from photo-induced fragmentation or oligomerization of SOA compounds
53 into more or less volatile products.^{12, 13} The direct photolysis of organic compounds¹⁴ or the secondary
54 oxidation by HO_x radicals (HO_2 and OH) deriving from photolysis¹⁵ explain the mass loss or decrease
55 in particle size as well as the VOCs release observed in several studies related to photochemical
56 processing of SOA.¹⁶⁻¹⁹ For example, in our previous work we have shown that secondary organic
57 material (SOM) is efficiently degraded by exposure to UV radiation producing CO , CO_2 , small
58 hydrocarbons,¹¹ as well as various oxygenated VOCs (OVOCs).^{16, 20, 21} (In this paper, we are using
59 “SOA” to refer to airborne particles, and “SOM” to the material formed by collecting bulk quantities
60 of SOA particles on a substrate.)

61 Relative humidity (RH) is an important environmental variable that effects not only physical
62 properties but also chemistry occurring inside the particles. It has been well established that SOA
63 particle viscosity depends strongly on RH.²²⁻²⁴ Related to that, RH has a strong influence on diffusion-
64 limited processes in SOA particles such as uptake or evaporation of chemical compounds or chemical
65 reactions. For example, Ye and coworkers found that SOA particles from toluene oxidation resist
66 exchange of semivolatile compounds at low relative humidity, but lose that resistance above 20%
67 RH.²⁵ Shiraiwa et al. showed that the uptake coefficient of ozone to protein films varies with relative

68 humidity due to the increase of the ozone diffusion coefficient with RH.²⁶ Similarly, Steimer et al.
69 (2016) demonstrated a strong relationship between the steady state reactivity of ozone with shikimic
70 acid and the estimated diffusivity of ozone as a function of relative humidity. Slade and Knopf
71 showed that increasing RH enhances the OH uptake in levoglucosan particles due to the faster
72 diffusion.²⁷ RH also is a key parameter controlling the rate of evaporation of OVOCs from SOA
73 particles as shown by Yli-Juuti et al.²⁸ The RH was found to influence the photodegradation of 2,4-
74 dinitrophenol through its effect on viscosity in several types of SOM including that generated by
75 oxidation of d-limonene by ozone.^{29, 30} They observed a faster photodegradation at high RH due to the
76 increase of the efficiency in the second-order degradation reactions, which are likely to be affected by
77 the diffusion limitations of the excited state, and therefore, by the viscosity.²⁹ Atmospheric models are
78 starting to take the RH-dependent viscosity into consideration and confirm that aerosol particles can
79 be liquid, semisolid or solid depending on the latitude, altitude and conditions, as predicted by
80 Shiraiwa et al.³¹ Our first goal is to understand the effect of RH on the photodegradation of SOA
81 compounds, which have not been previously explored in experiments. The results described below
82 suggest that the photodegradation rate estimates based on previous measurements under dry
83 conditions may be too conservative.¹⁶

84 Iron is emitted into the troposphere as minerals, as amorphous hydroxides, such as Fe(OH)₃, adsorbed
85 on clay minerals, organic matter, or carbonaceous particles or bound in salts. It may be released from
86 the particulate form by complexation or acidic dissolution into the aqueous phase.^{32, 33} Dissolved iron
87 is present in the atmosphere in two oxidation states, (II) and (III), which interconvert by various redox
88 processes. The work of Wang et al.³⁴ indicates that the iron can be highly concentrated in continental
89 aerosol particles near the surface of the Earth. For instance, in Europe the observed concentrations of
90 iron are between 0.1-1 $\mu\text{g m}^{-3}$ (~0.8-8% in molar ratio in SOA). A study from Moffet et al. (2012) has
91 shown that in urban outflow, all particles have organic matter dominated by carboxyl functionalities,
92 and, among them, 5% contain detectable Fe.³⁵ In the technique they used, the detection limit was
93 about 5% of iron in molar ratio. Saharan dust, urban particles, coal fly ash and oil fly ash contain iron
94 in the range from 3 to 9 % by weight.³³ The fraction of soluble Fe in desert dust typically goes from
95 values ~0.1% to up to ~80%.³⁶⁻³⁸ On the other hand, measurements of dissolved iron in rural or urban
96 atmospheric waters indicate concentrations ranging from 10^{-7} up to 10^{-2} M. Overall, dissolved iron
97 concentrations in aerosol particles vary broadly and range from micromolar up to an upper limit of
98 about 10%.

99 Depending on chemical parameters such as ionic strength, pH and concentration of involved
100 compounds, iron is present in the form of complexes with the organic and inorganic compounds in the
101 aerosol particles and cloud droplets.³³ Some of these complexes have strong ligand-to-metal charge
102 transfer (LMCT) bands in the UV and visible ranges of the solar spectrum. Excitation of these LMCT
103 bands in Fe(III) complexes leads to photoreduction of iron to Fe(II) and decomposition of the ligands
104 by free radical chemistry. Fe(III)-carboxylate complexes are well-known photoactive compounds in
105 atmospheric aerosol particles which drive LMCT transitions leading to the decarboxylation of the
106 ligands, being the major particle phase sink of carboxylate groups in the atmosphere.⁹ Even if SOM is
107 not light-absorbing by itself it can become photodegradable in presence of soluble Fe because of these
108 LMCT transitions. The degradation of the carboxylic groups is followed by the production of OVOCs
109 and CO₂,^{39, 40} which contribute to the particle mass loss. Iron can cycle between Fe(II) and Fe(III)
110 through HO_x radicals and H₂O₂ chemistry due to several redox reactions⁸ such as Fenton reactions.
111 Figure 1 shows some of the key processes involved in photochemistry of Fe/SOM mixtures, which
112 may produce OVOCs by various mechanisms including direct photolysis or reactions with HO_x

140 SOA was generated by oxidation of d-limonene (Sigma-Aldrich, 98%) with ozone in a ~ 20 L
141 Plexiglas flow cell in the absence of seed particles. No particles were produced in control experiments
142 with ozone only flowing through the cell, without d-limonene added. Pure oxygen at 0.5 L/min was
143 sent through an ozone generator and into the flow cell. Limonene was evaporated in a separate 4.5
144 L/min air flow using a syringe pump at 25 $\mu\text{L}/\text{hour}$ liquid flow rate. The flow of air containing
145 limonene was mixed with the O_3/O_2 flow at the entrance of the flow cell. The starting mixing ratios of
146 ozone and limonene were about 20 ppm and 10 ppm, respectively, and the reaction time in the flow
147 cell was about 4 min.

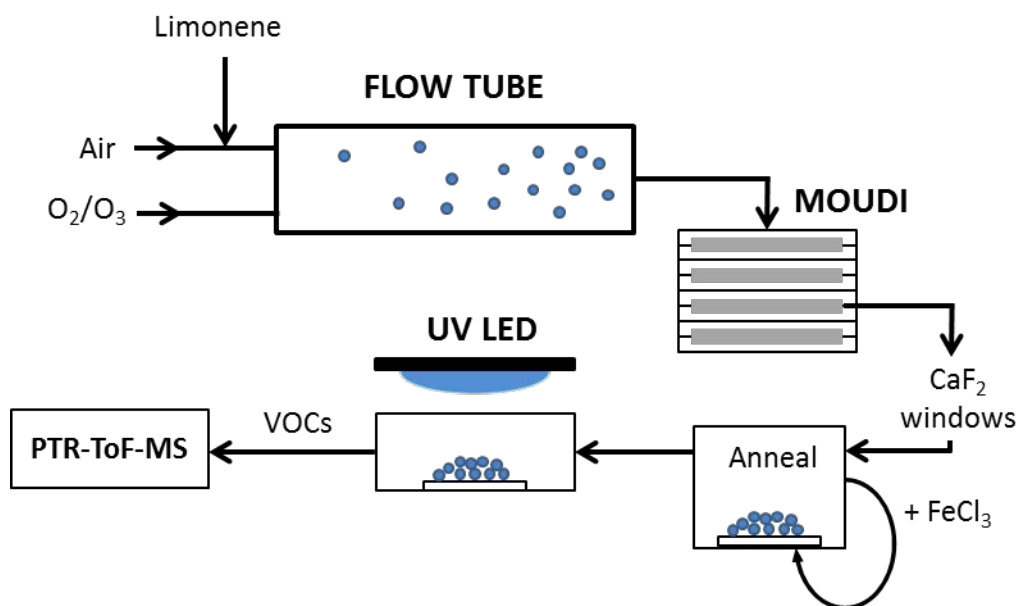
148 Particles were collected with a Micro-Orifice Uniform-Deposit Impactor (MOUDI, MSP Corp.
149 model 110-R) equipped with custom-made metal supporting rings to accommodate 2.54 cm diameter
150 CaF_2 windows as substrates instead of Teflon or foil filters. We typically collected hundreds of
151 micrograms of SOM per window; the largest amount was typically found on stages 8 (0.18-0.32 μm
152 particle size range) and 9 (0.10-0.18 μm particle size range), and these samples were used for the
153 experiments. In our previous experiments with d-limonene ozonolysis SOA, we found no dependence
154 of SOA particle chemical composition on particle size in the 0.05 to 0.5 μm range,⁴⁵ so we used
155 samples collected on stages 8 and 9 interchangeably. The window was then placed in a laboratory
156 oven overnight at 40 $^\circ\text{C}$ with ~10 L/min of purge air flowing over it in order to drive off higher
157 volatility species and help anneal the collected SOA particles into a more uniform SOM film on the
158 window. The main justification for this “annealing” procedure is that SOA produced by the
159 ozonolysis of alkenes contains unstable peroxide molecules that decompose on a time scale of
160 hours.^{10, 46} This decomposition produces volatile products that would interfere with the detection of
161 volatiles produced in the photodegradation experiments described below.¹⁶ In addition, semivolatile
162 species that partitioned into aerosol particles because of the unrealistically high concentrations in the
163 flow tube have a chance to evaporate making the volatility distribution of SOA compounds more
164 compatible with that of ambient aerosol particles. The annealed SOA samples can therefore be
165 regarded as particles that have been aged via spontaneous decomposition of peroxides but not by
166 photochemical processes. For the RH dependent experiments, we used the sample immediately after
167 annealing without further adjustments.

168 For the experiments with variable amounts of Fe(III), a certain volume ranging from 50 μL to 2000
169 μL of a solution of FeCl_3 in water (0.001M, pH = 5) was dropped on the window surface, and the
170 sample was placed again in the laboratory oven overnight under the same conditions as before.¹⁶ We
171 elected to use FeCl_3 as the Fe(III) source because it is highly soluble. While chloride anions are not
172 chemically inert and could be converted into chlorine atoms in reaction with OH, chloride anions are
173 ubiquitous in atmospheric particles, and it is reasonable to have them as part of the mixture. Even so,
174 the rate coefficient for the reaction between chloride and OH radicals⁴⁷ is around one order of
175 magnitude smaller than the one for the reaction between a usual SOA organic compound and OH.
176 Therefore the interference should be negligible. For larger volumes from 1000 μL up to 2000 μL , the
177 solution was applied in two additions to avoid spilling over the edges of the window. For volumes
178 lower than 500 μL , an additional droplet of water was added up to 500 μL to be sure that the solution
179 covered the entire window. For the control experiments, 500 μL of nanopure water was used instead
180 of the Fe-containing solution. The addition of liquid resulted in a redistribution of SOM on the CaF_2
181 window, resulting in a reduction in the film thickness in the center and a build-up of the material on
182 the edges. The material was redistributed due to an outflow created within the droplet while it was
183 evaporating due to the different evaporation rate in the edge compared with the one on the top of the
184 deposited droplet.⁴⁸ (In retrospect, it might have been better to prepare the samples differently, for
185 example by re-aerosolizing an aqueous solution of Fe(III) mixed with dissolved SOM and collecting

186 the resulting particles. Such experiments are planned for the future.) Because the CaF_2 window was
187 always fully covered by the deposited droplet, we assume that the fraction exposed to UV light was
188 always the same for every experiment and that the ratio $\text{Fe(III)}/\text{SOM}$ is homogeneous through the
189 sample after drying. Experiments with identical conditions of Fe(III) concentration, irradiation and
190 RH did not indicate a dependence of OVOCs release on the volume of solution used to deposit
191 Fe(III) .

192 The window was then placed into a custom-made glass flow cell with 0.2 L/min of purge air flowing
193 over the window. A UV-light emitting diode (Thorlabs, Inc. model M300L4) with a wavelength
194 centered at ~ 305 nm, a full width half-maximum of ~ 10 nm, and a power of 26 mW at 350 mA
195 current (measured with a Coherent Powermax PS19Q power sensor) was used to irradiate the particles
196 on the CaF_2 window. Based on the amount of the deposited material, and known mass absorption
197 coefficients of d-limonene ozonolysis SOA,⁴⁹ we estimated that the samples were optically thin, so the
198 UV intensity was approximately the same throughout the thickness of the sample. Although the
199 sample distribution on the surface was not uniform, as ascertained by the examination of the sample
200 under a microscope, all the material on the window was accessible to the UV radiation. For the
201 experiments with variable iron content dependence, the exposures to UV light were made either under
202 dry air conditions or at $55 \pm 2\%$ RH (measured with a Vaisala HMP330 humidity probe). For the
203 experiments related to the RH dependence of SOM decomposition, in which no Fe(III) was added to
204 the SOM sample, we exposed SOM to UV radiation under a wider range of RH values.

205 OVOCs in the flow exiting the photolysis cell were detected by a Proton Transfer Reaction Time-of-
206 Flight Mass Spectrometer (PTR-ToF-MS). Standard ion source conditions were used: $E/N = 130\text{-}135$
207 Td, $U_{\text{drift}} = 600\text{V}$, $T_{\text{drift}} = 60^\circ\text{C}$, and $P_{\text{drift}} \sim 2.2$ mbar. The PTR-ToF-MS was previously calibrated
208 under the same ion sources conditions with respect to several OVOCs, namely acetic acid, formic
209 acid, acetone and acetaldehyde by injecting known amounts of these compounds in a 5 m^3 chamber,
210 similar to a procedure described in Malecha and Nizkorodov.¹⁶ For experiments at different RH the
211 signal was normalized to take into account the RH dependence of the ion detection sensitivity.
212 Specifically, we evaluated the variation of the ionizing agents (H_3O^+ and $\text{H}_3\text{O}^+(\text{H}_2\text{O})$) with respect to
213 the experiments at dry conditions and we normalized the signal to those. We took into account the
214 different reactivity that the two ionizing agents have with the VOCs.^{50, 51} Additional details are
215 provided in the SI section.



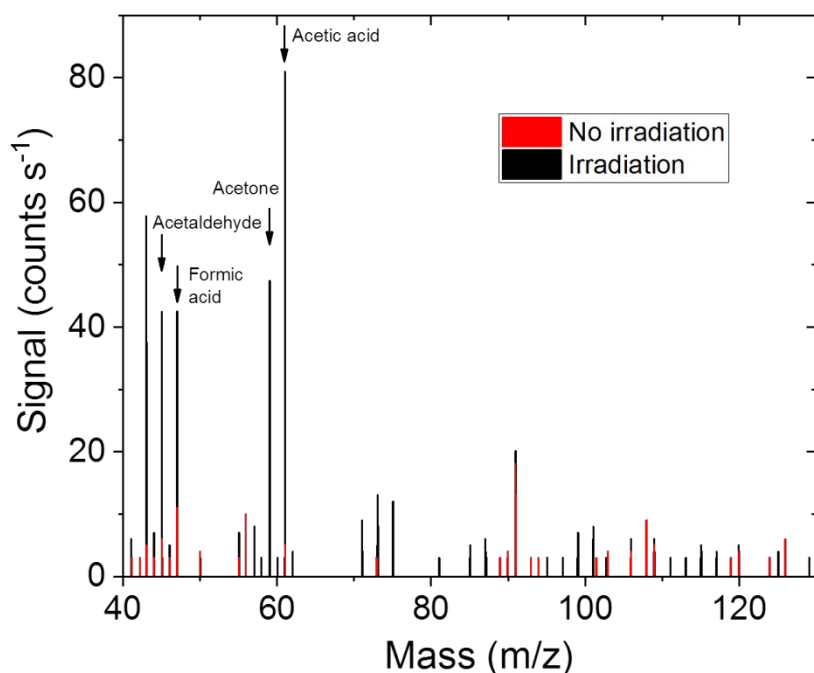
216

217 **Figure 2.** Diagram illustrating SOM preparation and UV exposure steps. SOA particles are produced
 218 by mixing a flow of air and O₂/O₃ with limonene in a flow tube. The particles are collected on CaF₂
 219 windows located in a MOUDI, and the particles are annealed. FeCl₃ is added for the iron content
 220 dependence experiments. After annealing at 40°C, samples are irradiated with a 305 nm UV-LED,
 221 and the OVOCs released are analyzed by a PTR-ToF-MS.

222 RESULTS AND DISCUSSION

223 Figure 3 shows PTR-ToF mass spectra of the air passing over the SOM before and during the UV
 224 irradiation. Upon irradiation, certain peaks increase indicating the production and release of the
 225 corresponding compounds from SOM. The major peaks that increase are detected at m/z 43.055
 226 (ketene, ethynol, or oxirene), m/z 45.034 (acetaldehyde), m/z 47.013 (formic acid), m/z 59.050
 227 (acetone, propanal, or allyl alcohol) and m/z 61.029 (acetic acid, glycoaldehyde, or methyl formate).
 228 Because of the inability of PTR-ToF-MS to distinguish structural isomers, the assignments cannot be
 229 made with certainty. However, because of chemical considerations about the possible mechanism of
 230 degradation, the m/z 45.034, 47.013, 59.050, and 61.029 peaks are assigned to acetaldehyde, formic
 231 acid, acetone and acetic acid, respectively. The peak at m/z 43.055 is likely a fragment of acetic acid.⁵²

232 Photolysis processes such as bond cleavage into free radicals, photoisomerization, H abstraction or
 233 photosensitization,² together with HO_x radical reactions, are the processes controlling the OVOC
 234 production. For example, acetone could be a product of degradation by Norrish type-II mechanisms,
 235 i.e., splitting of methyl terminated ketones. Acetic acid and formic acid could be produced by direct
 236 photolysis or by reaction of organics with HO_x radicals, which will react with organic by hydrogen
 237 abstraction and oxidation reactions which can lead to the cleavage of carbon chains. Additionally we
 238 rely on the LMCT reactions of iron complexes as additional source of CO₂ and OVOC by
 239 decarboxylation and further degradation of the organic radicals initially produced.



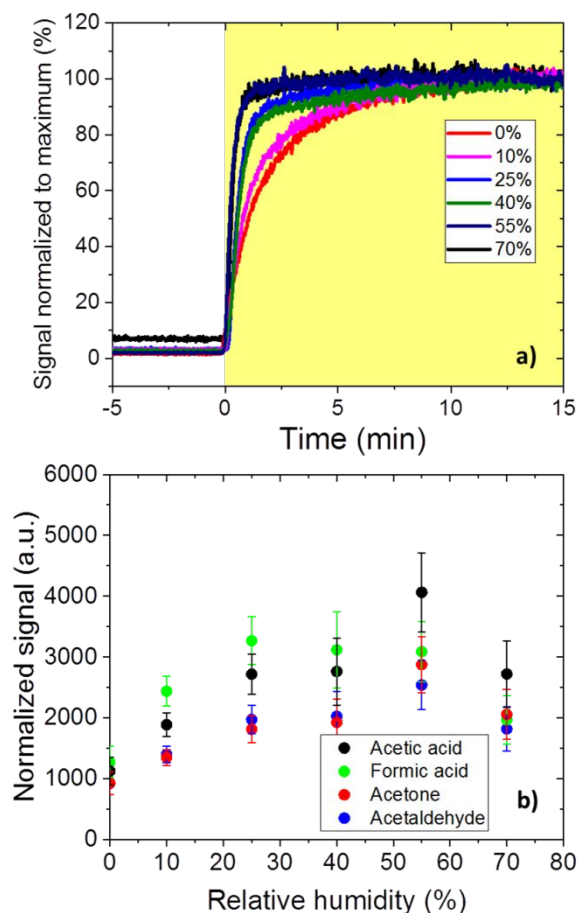
240

241 **Figure 3.** PTR-ToF-MS stick spectra of the OVOCs released from SOM at 0% RH, in the absence of
 242 iron before (red) and 10 minutes after starting irradiation (black) irradiation. The peaks of the sought
 243 molecule are pointed out.

244 *Effect of RH on samples without added Fe(III)*

245 Figure 4a shows the signal of acetaldehyde observed at different RH values. For ease of comparison,
 246 the signal was normalized to the maximal steady-state signal achieved during irradiation. The release
 247 of acetaldehyde levels off after about 15 minutes for dry conditions but the time needed to achieve the
 248 steady state becomes shorter for the experiments at higher RH (4 minutes for 70% RH). We attribute
 249 this faster time to establish steady state release of acetaldehyde at higher RH to an increased diffusion
 250 coefficient for acetaldehyde through SOM. (While we attribute our observations to the diffusion
 251 effects, we cannot exclude changes in the photochemical mechanisms arising, for example, from the
 252 hydrolysis of organic compounds at high RH.) The increased diffusivity would be caused by the
 253 decrease of viscosity with increasing water content in the film. Indeed, the viscosity of SOM prepared
 254 by ozonolysis of α -pinene⁵³ and d-limonene²⁹ has been shown to decrease with RH. The reported self-
 255 diffusion coefficients in SOM change widely with RH²²⁻²⁴ going from 10^{-22} - 10^{-20} $\text{cm}^2 \text{s}^{-1}$ at dry
 256 conditions to 10^{-9} - 10^{-7} $\text{cm}^2 \text{s}^{-1}$ at high RH (80-90% RH) while the diffusion coefficient of water in α -
 257 pinene SOA varies from 10^{-11} - 10^{-10} $\text{cm}^2 \text{s}^{-1}$ at dry conditions to 10^{-8} - 10^{-6} $\text{cm}^2 \text{s}^{-1}$ at high RH.

258



259

260 **Figure 4.** (a) Signal of acetaldehyde normalized to the maximum of the signal for each sample upon
 261 irradiation (shaded zone) at several values of RH. (b) Signal of OVOCs upon UV irradiation
 262 corresponding to the total OVOC flux and multiplied by the flow in mL/min for SOM samples versus
 263 relative humidity (%). The error bars represent the standard deviation resulting from 2 or 3
 264 experiments.

265 Figure 4b shows the dependence of release of several OVOCs on RH. Each data point is the average
 266 of 2 or 3 replica experiments. Since the ionization efficiency of certain low-proton-affinity VOCs
 267 (such as benzene,⁵⁴ monoterpenes,⁵⁵ and formaldehyde⁵⁶) is sensitive to RH, we corrected for the RH-
 268 dependent ionization efficiency in the PTR as described in the SI. For the species of interest, these
 269 corrections were very small. In the data shown in Fig. 4b, the signal was normalized by the total mass
 270 of the SOM assuming that the amount of emitted OVOC should be directly proportional to the SOM
 271 mass (the SOM samples were optically thin, so such normalization is appropriate). The signal was
 272 further multiplied by the total gas flow through the sample in order to correct for the dilution with
 273 different gas flows used in different experiments. With this normalization method, the magnitude of
 274 the normalized signal is proportional to the actual OVOC flux out of the material. The data were taken
 275 from the time period where the release reaches the maximum which was different for different
 276 humidity conditions, as shown in Fig. 4a.

277 The release of every compound shown in Fig. 4b increases with RH from 0% to 40-55 % RH. There
 278 are two possible explanations for this. Firstly, certain photochemical reactions are suppressed in
 279 viscous SOA, especially the ones involving secondary reactions of long-lived electronically excited
 280 molecules.²⁹ Secondly, since it takes OVOCs longer to diffuse through the SOM at lower RH, the

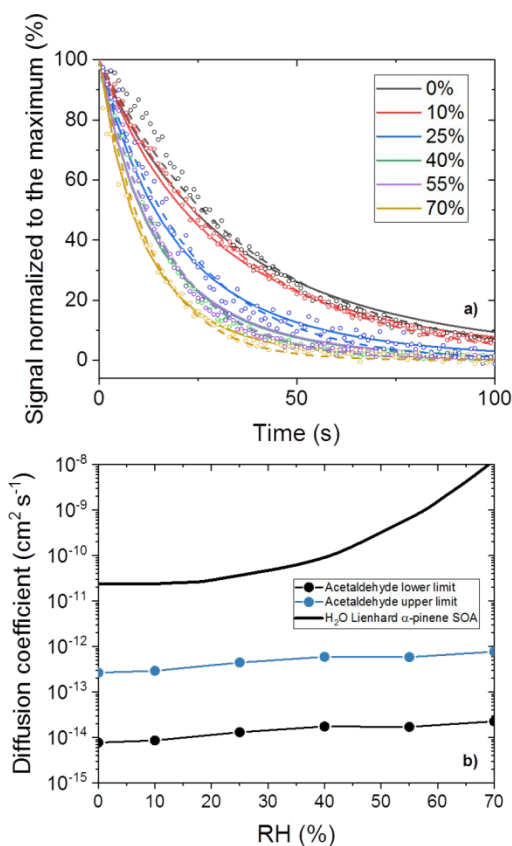
281 probability that they are degraded by secondary free-radical driven reactions before they get out of the
282 material increases.

283 From 55% RH to 70% RH the rate of OVOC release appears to decrease by more than 25% (although
284 we have only one data point that shows this trend). This could be a result of a dilution effect: as the
285 water activity in the SOM increases the concentrations of all other reactants decrease. Based on the
286 work of Virkkula and coworkers,⁵⁷ the concentration of water in d-limonene SOA goes up to 7 M at
287 80% RH, and it could be even higher in the presence of hygroscopic FeCl₃. Previous research has
288 shown that oxygen solubility in organic solvents, such ethanol, propanol or carboxylic acids, is higher
289 than in water.⁵⁸ Therefore, we assume that oxygen solubility also decreases upon increasing water
290 activity meaning that HO_x radicals deriving from photolysis of SOM will be produced less efficiently
291 since the precursor molecule (O₂) is less concentrated and subsequently OVOC production will be
292 decreased. (HO_x radicals could also be produced by the photolysis of peroxides in d-limonene
293 ozonolysis SOM but the lifetime of peroxides in this SOM is known to be around 6 hours,⁴⁶ so most
294 of them should be already degraded by the annealing procedure done before the measurement.) The
295 decrease of the concentration of both organic reactants and oxygen at higher RH should result in a
296 decrease of second order reaction rates. Thus, the OVOC release is expected to get smaller with
297 increasing RH. Similar dependence on RH, featuring a maximum at certain RH level, was observed in
298 the HO₂ release in previous work.⁴

299 We estimated the diffusion coefficient of acetaldehyde at different values of RH based on the decay of
300 its concentration in the flow after switching off the UV light (Figure 5). We developed a kinetic multi-
301 layer model by means of the diffusion equation (Eq. 1), which provides a depth-resolved description
302 of mass transport and release in films as a function of time, dividing our film in 30 equally thick
303 layers. A detailed description of the model is provided in the SI. The diffusion is considered
304 throughout the film by applying the diffusion equation to every layer. Since the gas flow over the film
305 is fast (on the order of hundreds of mL per minute), we assume that the gas phase concentration of
306 acetaldehyde next to the surface plays no role in the equilibrium between condensed and gas phase.
307 Therefore, the release is described as the diffusion into a gas layer, where the concentration is
308 negligible. We estimated the thickness of the sample assuming that the density of the SOM is 1.5
309 g/cm³.⁵⁹

310
$$\frac{\partial C}{\partial t} = D \frac{\partial^2 C}{\partial x^2} \quad (1)$$

311 We optimized the values of the diffusion coefficients at different RH by fitting the release predicted
312 by the model to the observed decay of acetaldehyde after switching off lights as shown in Fig. 5a. We
313 note that the initial concentration profile in the film may change the release. Therefore, we tested the
314 sensitivity of two initial concentration profiles on the diffusion coefficient parameter to reproduce our
315 data: i) uniform initial concentration profile is flat throughout the film (which is consistent with the
316 optically thin samples used in this work, with the UV radiation penetrating through the entire film)
317 and ii) linear initial concentration profile where its maximum concentration is at the bottom of the
318 film and zero at the surface (a conceivable scenario after prolonged irradiation). These two different
319 scenarios should provide a lower (i) and upper (ii) limit set of predicted diffusion coefficients
320 respectively.



321

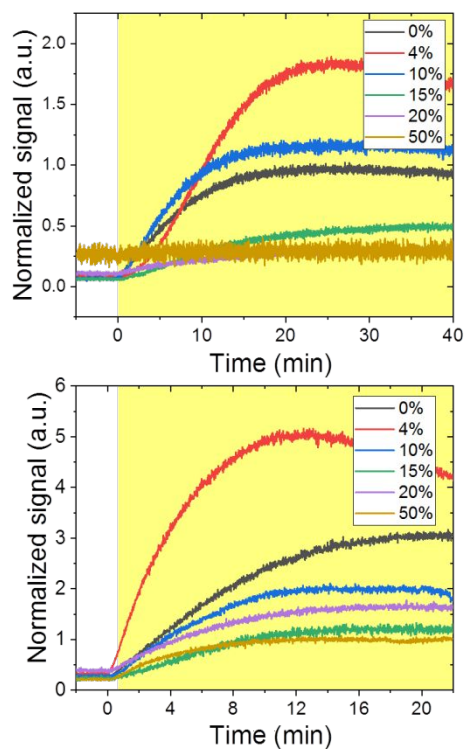
322 **Figure 5.** (a) Signal of acetaldehyde after irradiation background-subtracted and normalized to the
 323 maximum of the signal for each sample upon irradiation (symbols) as a function of RH. Predictions
 324 by the diffusion model with upper and lower limits for the diffusion coefficient are shown as dashed
 325 and solid lines, respectively. (b) Diffusion coefficients predicted by the model for acetaldehyde as a
 326 function of RH, with the upper (blue) and lower (black) limits shown as blue and black symbols,
 327 respectively. The black line corresponds to the water diffusion coefficient in α -pinene SOA as
 328 measured by Lienhard et al.⁶⁰

329 The trend of the calculated diffusion coefficients follows the expected trend, i.e., diffusion
 330 coefficients increasing with RH. The calculated upper limit diffusion coefficients of acetaldehyde are
 331 two or three orders of magnitude at low RH and four or five orders of magnitude at high RH lower
 332 than the diffusion coefficients of water in alpha-pinene SOA measured previously by Lienhard et al.⁶⁰
 333 as showed in Fig. 5. The molecule of acetaldehyde is larger than the molecule of water so, based on
 334 the Stokes-Einstein equation, we would expect water to diffuse only around two times faster than
 335 acetaldehyde. However, the Stokes-Einstein equation performs poorly for molecules of this size,⁶¹ so
 336 quantitative comparison is not possible. But as the upper limit values for the acetaldehyde diffusion
 337 coefficients in Figure 5 are closer to the reported values for water, they are probably more
 338 representative of the actual diffusion coefficients. The relative change of D between 0 and 70 % RH is
 339 a factor of 2-3 while a range of about one or two orders of magnitude is observed for $D_{\text{H}_2\text{O}}$ in SOA^{60, 62}
 340 and a range of about 9 to 10 orders of magnitude is observed for D_{org} in sucrose.⁶³ A possible
 341 explanation for this would be that the steady-state profile of the concentration of acetaldehyde in
 342 limonene SOA while irradiation is flat at low RH (lower limit prediction) and it will have a gradient at
 343 high RH (upper limit prediction). This latter situation will lead to a difference of D of about two
 344 orders of magnitude from low RH and high RH..

345 **Effect of added Fe(III)**

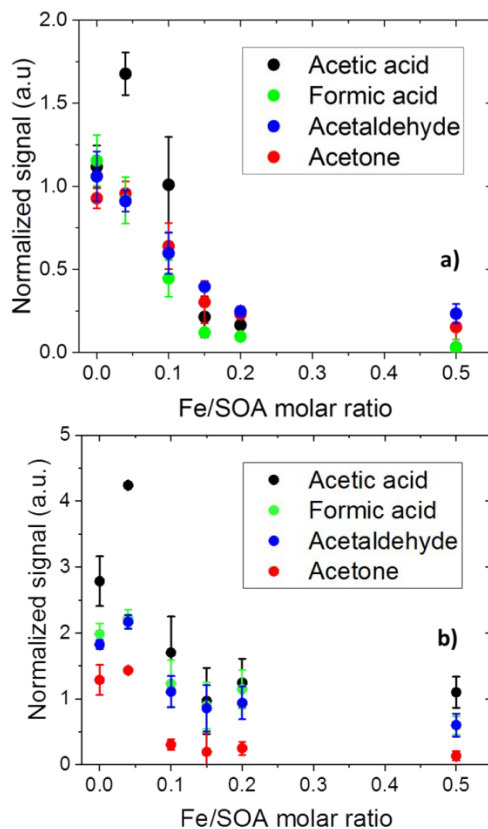
346 Figure 6 shows the PTR-ToF-MS time-dependent signal of acetic acid released under irradiation
347 under dry conditions (a) and at 55% RH (b). The signal was normalized by the initial dry mass of
348 SOM on the substrate (it was not corrected for the RH-dependent ionization efficiency because only
349 signals at the same RH are compared to each other). Different traces correspond to different mole
350 fractions of added Fe(III) (estimated assuming an average molar mass of 200 g/mol for SOM
351 compounds). The release reaches a maximum around 30 minutes after the start of the irradiation, and
352 after that the release drops slowly, and finally drops to the baseline level after several hours of UV
353 exposure (not shown). At 55% RH, the maximum signal is reached earlier than under dry conditions
354 because the diffusion of the OVOCs through SOM is faster at higher RH, as discussed above, and the
355 steady state release is reached earlier. The release of other compounds (acetaldehyde, formic acid, and
356 acetone) shows the same trend as acetic acid.

357 Figure 7 shows the average of the normalized signal of the 4 OVOCs under dry conditions (a) and at
358 55% RH (b). To account for the faster appearance of the signal in humidified air, the averaging period
359 is 2000 s - 2500 s (33.3 min – 46.7 min) for dry conditions, and 750 s – 1000 s (12.5 – 16.7 min) at
360 55% RH. Contrary to our expectations that the presence of Fe should accelerate photodegradation of
361 SOM, there is a general decreasing trend in the signal of OVOC photoproducts with the relative
362 amount of added Fe. This overall decreasing trend cannot be explained by the differences in the
363 absorption coefficients of the samples because the samples were in fact more absorbing at higher Fe
364 fractions (however, we have not corrected for the change in the absorption coefficient in this work).
365 The trend is not linear, however. At 55% RH, the release of all OVOC is higher for samples with 4%
366 of Fe(III) compared to samples without added Fe. Above that fraction (and above 10% for acetone
367 and acetic acid), OVOC release drops below that of SOM without Fe added. Then at higher Fe(III)
368 concentrations, the release is strongly suppressed. Under dry conditions, acetic acid and perhaps
369 acetone follow a similar trend with a maximum emission at 4% Fe(III), and decreasing at higher
370 Fe(III) concentrations. For acetaldehyde and formic acid there is a steady decrease of the signal as the
371 Fe(III) concentration is increasing. At 55% RH, all species exhibit first increased release with
372 increasing Fe(III) content, and then a decrease for higher Fe(III) additions. We suspect that two
373 competing effects maybe at work, one enhancing the OVOC release at low Fe(III) concentrations and
374 suppressing it at high Fe(III) concentrations.



375

376 **Figure 6.** PTR-ToF-MS signal of acetic acid released upon UV irradiation for SOM samples versus
377 time at different mole fractions of added FeCl₃ (specified with % values in each panel) under dry
378 conditions (a) and at 55% RH (b). The yellow-shaded zone indicates the irradiation time. Signals from
379 different samples were normalized to the total mass of the sample.



380

381 **Figure 7.** Peak intensities of signals from acetic acid, formic acid, acetaldehyde and acetone
 382 normalized to the total mass of the sample for SOM samples versus Fe/SOA molar ratio under dry
 383 conditions (a) and at 55% RH (b). The error bars represent the standard deviation resulting from 2 or 3
 384 repeated experiments.

385 The enhancement in the release of OVOCs at low Fe(III) concentrations may result from increased
 386 OVOC production from the photolysis of iron carboxylate complexes likely produced after adding
 387 Fe(III) to SOM, as illustrated in Figure 1. This is in agreement with the work of Hems et al.⁶⁴ which
 388 found that the OH production from the photodegradation of SOA compounds by themselves is slower
 389 than the one promoted by iron carboxylate complexes formed between iron and SOA material at low
 390 Fe/SOA ratio (~0.3%). The enhancement in OVOC release can be due to i) increase of the HO_x
 391 radical production inside SOM and ii) the direct photolysis of iron carboxylate complexes. We also
 392 cannot discard a possibility that the chloride anions present in the samples are not playing a role in the
 393 photochemistry – they could potentially be converted into highly reactive chlorine atoms by reactions
 394 with OH inside SOM. Our experiments cannot differentiate between these possibilities.

395 The decrease of the OVOC release at high iron concentration may be the result of the presence of
 396 incompletely complexed Fe in the condensed phase, i.e., not with all coordination sites occupied by
 397 the SOA carboxylic ligands. Instead of driving LMCT transitions, incompletely complexed iron could
 398 be cycling between Fe(III) and Fe(II) (Fig.1) turning HO_x radicals into water and oxygen and making
 399 them unavailable to oxidize SOA compounds into OVOCs.

400 CONCLUSIONS AND ATMOSPHERIC IMPLICATIONS

401 This work reveals that RH will play an important role in the OVOC release from SOA induced by
 402 photolysis of the compounds presents in SOA. In the work of Malecha and Nizkorodov (2016), they

403 estimated the emission of OVOC coming from the photolysis of several SOA under dry conditions
404 and they predicted that SOA particles may lose at least ~1% of their mass over 24 hours during
405 summertime conditions in Los Angeles, California. We claim that, under more realistic relative
406 humidity conditions (~50%), the mass loss experienced by SOA particles may be up to 2 to 4 times
407 higher than what was estimated in the work of Malecha and Nizkorodov.¹⁶ We propose that all future
408 photodegradation studies of SOA should be done under humid conditions to more accurately estimate
409 the rate of mass loss from the particles. To explain the assumption that D varies over several orders of
410 magnitude while increasing RH from 0% to 70%, we suggest the presence of OVOCs concentration
411 gradients taking place over a range of hundreds of nanometers in aerosol particles during photolysis.
412 When photolysis rates are not too high, these gradients are presumably kept in a situation close to
413 steady-state in atmospheric aerosol particles but they can develop while the particles age. Their spatial
414 extent depends on humidity conditions, nature of the SOM and nature of the diffusing molecule. The
415 diffusion coefficient of acetaldehyde in limonene SOA is the range from 10^{-14} to 10^{-12} $\text{cm}^2 \text{s}^{-1}$.

416 The second conclusion of this work is that iron influences the OVOC generation and release during
417 UV irradiation of SOA particles. For atmospherically relevant conditions of humidity and iron content
418 (up to 4% of iron molar ratio), OVOC release will be slightly enhanced likely due to the efficient
419 photo-degradation of iron carboxylate complexes. At higher iron content a surprising suppression of
420 the photodegradation is observed, although such high concentrations are unlikely in realistic
421 atmospheric particles. As described in the introduction, dissolved iron concentrations in aerosol
422 particles vary broadly and range from micromolar up to an upper limit of about 10%. Our findings
423 point out that OVOC production and release is strongly influenced by iron in iron-containing
424 particles, with the sign and magnitude of the effects being dependent on the concentration and
425 conditions.

426 ASSOCIATED CONTENT

427 Supporting Information.

428 The Supporting Information is available free of charge on the ACS Publications website at DOI:
429 XXXX. It describes the procedure for accounting for RH dependence of the PTR-ToF-MS ionization
430 efficiency, and the kinetic multi-layer modelling of OVOCs diffusing through the photolyzed SOM
431 sample.

432 AUTHOR INFORMATION

433 Corresponding Author

434 *Phone: +1-949-824-1262. Fax: +1-949-824-8671. Email: nizkorod@uci.edu

435 ORCID

436 Pablo Corral Arroyo: 0000-0003-4090-1623

437 Kurtis T. Malecha: 0000-0002-1438-7440

438 Markus Ammann: 0000-0001-5922-9000

439 Sergey A. Nizkorodov: 0000-0003-0891-0052

440 ResearcherID

441 Pablo Corral Arroyo: M-4878-2018

442 Kurtis T. Malecha: Q-4687-2016

443 Markus Ammann: E-4576-2011

444 Sergey A. Nizkorodov: I-4120-2014

445 Notes

446 The authors declare no competing financial interests.

447 ACKNOWLEDGMENTS

448 We would like to thank Peter A. Alpert for helpful discussions and support. P.C.A. and M.A.
449 appreciate support by the Swiss National Science Foundation (grant no 163074). K.T.M. thanks the
450 National Science Foundation (NSF) for support from the Graduate Research Fellowship Program.
451 S.A.N. thanks a grant from the US Department of Energy (DE-SC0018349) for the support. The PTR-
452 ToF-MS was acquired with the NSF grant MRI-0923323.

453 References:

- 454 1. Poschl, U., Atmospheric aerosols: composition, transformation, climate and health effects.
455 *Angewandte Chemie* **2005**, *44*, (46), 7520-40.
- 456 2. George, C.; Ammann, M.; D'Anna, B.; Donaldson, D. J.; Nizkorodov, S. A., Heterogeneous
457 Photochemistry in the Atmosphere. *Chem. Rev.* **2015**, *115*, (10), 4218-4258.
- 458 3. Shiraiwa, M.; Yee, L. D.; Schilling, K. A.; Loza, C. L.; Craven, J. S.; Zuend, A.; Ziemann, P. J.;
459 Seinfeld, J. H., Size distribution dynamics reveal particle-phase chemistry in organic aerosol
460 formation. *Proc. Natl. Acad. Sci. U. S. A.* **2013**, *110*, (29), 11746-11750.
- 461 4. González Palacios, L.; Corral Arroyo, P.; Aregahegn, K. Z.; Steimer, S. S.; Bartels-Rausch, T.;
462 Nozière, B.; George, C.; Ammann, M.; Volkamer, R., Heterogeneous photochemistry of imidazole-2-
463 carboxaldehyde: HO₂ radical formation and aerosol growth. *Atmos. Chem. Phys.* **2016**, *16*, (18),
464 11823-11836.
- 465 5. Sharpless, C. M.; Blough, N. V., The importance of charge-transfer interactions in
466 determining chromophoric dissolved organic matter (CDOM) optical and photochemical properties.
467 *Environ Sci Process Impacts* **2014**, *16*, (4), 654-71.
- 468 6. Smith, J. D. S.; Yu, L.; Zhang, Q.; Anastasio, C., Secondary organic aerosol production from
469 aqueous reactions of atmospheric phenols with an organic triplet excited state. *Environmental*
470 *science & technology* **2014**, *48*, (2), 1049-57.
- 471 7. Aregahegn, K. Z.; Nozière, B.; George, C., Organic aerosol formation photo-enhanced by the
472 formation of secondary photosensitizers in aerosols. *Faraday Discuss.* **2013**, *165*, 123-134.
- 473 8. Herrmann, H.; Ervens, B.; Jacobi, H. W.; Wolke, R.; Nowacki, P.; Zellner, R., CAPRAM2.3: A
474 chemical aqueous phase radical mechanism for tropospheric chemistry. *J. Atmos. Chem.* **2000**, *36*,
475 (3), 231-284.
- 476 9. Weller, C.; Tilgner, A.; Brauer, P.; Herrmann, H., Modeling the impact of iron-carboxylate
477 photochemistry on radical budget and carboxylate degradation in cloud droplets and particles.
478 *Environmental science & technology* **2014**, *48*, (10), 5652-9.
- 479 10. Krapf, M.; El Haddad, I.; Bruns, E. A.; Molteni, U.; Daellenbach, K. R.; Prevot, A. S. H.;
480 Baltensperger, U.; Dommen, J., Labile Peroxides in Secondary Organic Aerosol. *Chem* **2016**, *1*, (4),
481 603-616.
- 482 11. Mang, S. A.; Henricksen, D. K.; Bateman, A. P.; Andersen, M. P. S.; Blake, D. R.; Nizkorodov, S.
483 A., Contribution of carbonyl photochemistry to aging of atmospheric secondary organic aerosol. *J.*
484 *Phys. Chem. A* **2008**, *112*, (36), 8337-8344.

- 485 12. Henry, K. M.; Donahue, N. M., Photochemical Aging of alpha-Pinene Secondary Organic
486 Aerosol: Effects of OH Radical Sources and Photolysis. *J. Phys. Chem. A* **2012**, *116*, (24), 5932-5940.
- 487 13. Romonosky, D. E.; Li, Y.; Shiraiwa, M.; Laskin, A.; Laskin, J.; Nizkorodov, S. A., Aqueous
488 Photochemistry of Secondary Organic Aerosol of alpha-Pinene and alpha-Humulene Oxidized with
489 Ozone, Hydroxyl Radical, and Nitrate Radical. *J. Phys. Chem. A* **2017**, *121*, (6), 1298-1309.
- 490 14. Bateman, A. P.; Nizkorodov, S. A.; Laskin, J.; Laskin, A., Photolytic processing of secondary
491 organic aerosols dissolved in cloud droplets. *Physical Chemistry Chemical Physics* **2011**, *13*, (26),
492 12199-12212.
- 493 15. Kroll, J. H.; Smith, J. D.; Che, D. L.; Kessler, S. H.; Worsnop, D. R.; Wilson, K. R., Measurement
494 of fragmentation and functionalization pathways in the heterogeneous oxidation of oxidized organic
495 aerosol. *Physical Chemistry Chemical Physics* **2009**, *11*, (36), 8005-8014.
- 496 16. Malecha, K. T.; Nizkorodov, S. A., Photodegradation of Secondary Organic Aerosol Particles
497 as a Source of Small, Oxygenated Volatile Organic Compounds. *Environmental science & technology*
498 **2016**, *50*, (18), 9990-7.
- 499 17. Daumit, K. E.; Carrasquillo, A. J.; Sugrue, R. A.; Kroll, J. H., Effects of Condensed-Phase
500 Oxidants on Secondary Organic Aerosol Formation. *J. Phys. Chem. A* **2016**, *120*, (9), 1386-1394.
- 501 18. Wong, J. P. S.; Zhou, S. M.; Abbatt, J. P. D., Changes in Secondary Organic Aerosol
502 Composition and Mass due to Photolysis: Relative Humidity Dependence. *J. Phys. Chem. A* **2015**, *119*,
503 (19), 4309-4316.
- 504 19. Epstein, S. A.; Blair, S. L.; Nizkorodov, S. A., Direct Photolysis of a-Pinene Ozonolysis
505 Secondary Organic Aerosol: Effect on Particle Mass and Peroxide Content. *Environmental science &*
506 *technology* **2014**, *48*, (19), 11251-11258.
- 507 20. Pan, X.; Underwood, J. S.; Xing, J. H.; Mang, S. A.; Nizkorodov, S. A., Photodegradation of
508 secondary organic aerosol generated from limonene oxidation by ozone studied with chemical
509 ionization mass spectrometry. *Atmos. Chem. Phys.* **2009**, *9*, (12), 3851-3865.
- 510 21. Walser, M. L.; Park, J.; Gomez, A. L.; Russell, A. R.; Nizkorodov, S. A., Photochemical aging of
511 secondary organic aerosol particles generated from the oxidation of d-limonene. *J. Phys. Chem. A*
512 **2007**, *111*, (10), 1907-1913.
- 513 22. Berkemeier, T.; Steimer, S. S.; Krieger, U. K.; Peter, T.; Poschl, U.; Ammann, M.; Shiraiwa, M.,
514 Ozone uptake on glassy, semi-solid and liquid organic matter and the role of reactive oxygen
515 intermediates in atmospheric aerosol chemistry. *Phys. Chem. Chem. Phys.* **2016**, *18*, (18), 12662-74.
- 516 23. Song, Y. C.; Haddrell, A. E.; Bzdek, B. R.; Reid, J. P.; Bannan, T.; Topping, D. O.; Percival, C.;
517 Cai, C., Measurements and Predictions of Binary Component Aerosol Particle Viscosity. *J. Phys.*
518 *Chem. A* **2016**, *120*, (41), 8123-8137.
- 519 24. Lienhard, D. M.; Huisman, A. J.; Bones, D. L.; Te, Y. F.; Luo, B. P.; Krieger, U. K.; Reid, J. P.,
520 Retrieving the translational diffusion coefficient of water from experiments on single levitated
521 aerosol droplets. *Physical chemistry chemical physics : PCCP* **2014**, *16*, (31), 16677-83.
- 522 25. Ye, Q.; Robinson, E. S.; Ding, X.; Ye, P.; Sullivan, R. C.; Donahue, N. M., Mixing of secondary
523 organic aerosols versus relative humidity. *Proc. Natl. Acad. Sci. U. S. A.* **2016**.
- 524 26. Shiraiwa, M.; Ammann, M.; Koop, T.; Poschl, U., Gas uptake and chemical aging of semisolid
525 organic aerosol particles. *Proc. Natl. Acad. Sci. U. S. A.* **2011**, *108*, (27), 11003-11008.
- 526 27. Slade, J. H.; Knopf, D. A., Multiphase OH oxidation kinetics of organic aerosol: The role of
527 particle phase state and relative humidity. *Geophysical Research Letters* **2014**, *41*, (14), 5297-5306.
- 528 28. Yli-Juuti, T.; Pajunoja, A.; Tikkanen, O. P.; Buchholz, A.; Faiola, C.; Vaisanen, O.; Hao, L. Q.;
529 Kari, E.; Perakyla, O.; Garmash, O.; Shiraiwa, M.; Ehn, M.; Lehtinen, K.; Virtanen, A., Factors
530 controlling the evaporation of secondary organic aerosol from alpha-pinene ozonolysis. *Geophys.*
531 *Res. Lett.* **2017**, *44*, (5), 2562-2570.
- 532 29. Hinks, M. L.; Brady, M. V.; Lignell, H.; Song, M. J.; Grayson, J. W.; Bertram, A. K.; Lin, P.;
533 Laskin, A.; Laskin, J.; Nizkorodov, S. A., Effect of viscosity on photodegradation rates in complex
534 secondary organic aerosol materials. *Phys. Chem. Chem. Phys.* **2016**, *18*, (13), 8785-8793.

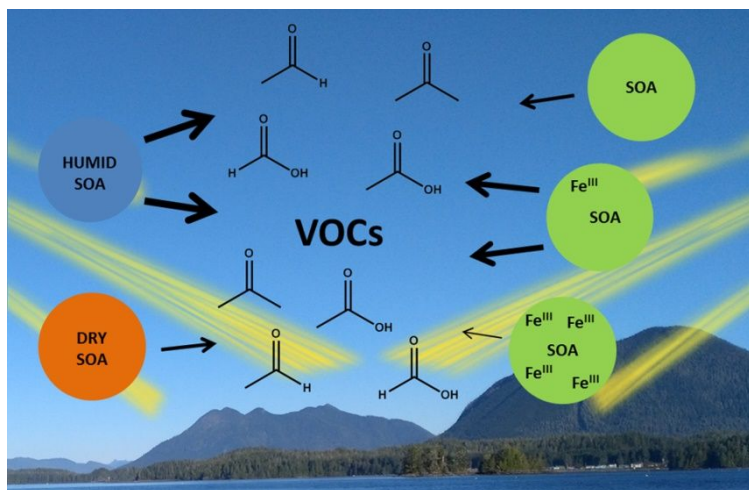
- 535 30. Lignell, H.; Hinks, M. L.; Nizkorodov, S. A., Exploring matrix effects on photochemistry of
536 organic aerosols. *Proc. Natl. Acad. Sci. U. S. A.* **2014**, *111*, (38), 13780-13785.
- 537 31. Shiraiwa, M.; Li, Y.; Tsimpidi, A. P.; Karydis, V. A.; Berkemeier, T.; Pandis, S. N.; Lelieveld, J.;
538 Koop, T.; Poschl, U., Global distribution of particle phase state in atmospheric secondary organic
539 aerosols. *Nature communications* **2017**, *8*, 7.
- 540 32. Cwiertny, D. M.; Hunter, G. J.; Pettibone, J. M.; Scherer, M. M.; Grassian, V. H., Surface
541 Chemistry and Dissolution of alpha-FeOOH Nanorods and Microrods: Environmental Implications of
542 Size-Dependent Interactions with Oxalate. *J. Phys. Chem. C* **2009**, *113*, (6), 2175-2186.
- 543 33. Deguillaume, L.; Leriche, M.; Desboeufs, K.; Mailhot, G.; George, C.; Chaumerliac, N.,
544 Transition metals in atmospheric liquid phases: Sources, reactivity, and sensitive parameters.
545 *Chemical reviews* **2005**, *105*, (9), 3388-3431.
- 546 34. Wang, R.; Balkanski, Y.; Boucher, O.; Bopp, L.; Chappell, A.; Ciais, P.; Hauglustaine, D.;
547 Peñuelas, J.; Tao, S., Sources, transport and deposition of iron in the global atmosphere. *Atmos.*
548 *Chem. Phys.* **2015**, *15*, (11), 6247-6270.
- 549 35. Moffet, R. C.; Furutani, H.; Rödel, T. C.; Henn, T. R.; Sprau, P. O.; Laskin, A.; Uematsu, M.;
550 Gilles, M. K., Iron speciation and mixing in single aerosol particles from the Asian continental
551 outflow. *Journal of Geophysical Research: Atmospheres* **2012**, *117*, (D7), D07204.
- 552 36. Journet, E.; Desboeufs, K. V.; Caquineau, S.; Colin, J. L., Mineralogy as a critical factor of dust
553 iron solubility. *Geophysical Research Letters* **2008**, *35*, (7), 5.
- 554 37. Mahowald, N. M.; Engelstaedter, S.; Luo, C.; Sealy, A.; Artaxo, P.; Benitez-Nelson, C.; Bonnet,
555 S.; Chen, Y.; Chuang, P. Y.; Cohen, D. D.; Dulac, F.; Herut, B.; Johansen, A. M.; Kubilay, N.; Losno, R.;
556 Maenhaut, W.; Paytan, A.; Prospero, J. A.; Shank, L. M.; Siefert, R. L., Atmospheric Iron Deposition:
557 Global Distribution, Variability, and Human Perturbations. *Annu. Rev. Mar. Sci.* **2009**, *1*, 245-278.
- 558 38. Shi, Z. B.; Krom, M. D.; Jickells, T. D.; Bonneville, S.; Carslaw, K. S.; Mihalopoulos, N.; Baker, A.
559 R.; Benning, L. G., Impacts on iron solubility in the mineral dust by processes in the source region and
560 the atmosphere: A review. *Aeolian Res.* **2012**, *5*, 21-42.
- 561 39. Weller, C.; Horn, S.; Herrmann, H., Photolysis of Fe(III) carboxylate complexes: Fe(II)
562 quantum yields and reaction mechanisms. *Journal of Photochemistry and Photobiology A: Chemistry*
563 **2013**, *268*, 24-36.
- 564 40. Abrahamson, H. B.; Rezvani, A. B.; Brushmiller, J. G., Photochemical and spectroscopic
565 studies of complexes of iron(III) with citric acid and other carboxylic acids. *Inorg. Chim. Acta* **1994**,
566 *226*, (1-2), 117-127.
- 567 41. Wentworth, G. R.; Al-Abadleh, H. A., DRIFTS studies on the photosensitized transformation
568 of gallic acid by iron(III) chloride as a model for HULIS in atmospheric aerosols. *Physical Chemistry*
569 *Chemical Physics* **2011**, *13*, (14), 6507-6516.
- 570 42. Nguyen, T. B.; Coggon, M. M.; Flagan, R. C.; Seinfeld, J. H., Reactive Uptake and Photo-
571 Fenton Oxidation of Glycolaldehyde in Aerosol Liquid Water. *Environ. Sci. Technol.* **2013**, *47*, (9),
572 4307-4316.
- 573 43. Thomas, D. A.; Coggon, M. M.; Lignell, H.; Schilling, K. A.; Zhang, X.; Schwantes, R. H.; Flagan,
574 R. C.; Seinfeld, J. H.; Beauchamp, J. L., Real-Time Studies of Iron Oxalate-Mediated Oxidation of
575 Glycolaldehyde as a Model for Photochemical Aging of Aqueous Tropospheric Aerosols. *Environ. Sci.*
576 *Technol.* **2016**, *50*, (22), 12241-12249.
- 577 44. Styler, S. A.; Donaldson, D. J., Heterogeneous Photochemistry of Oxalic Acid on Mauritanian
578 Sand and Icelandic Volcanic Ash. *Environmental science & technology* **2012**, *46*, (16), 8756-8763.
- 579 45. Bateman, A. P.; Nizkorodov, S. A.; Laskin, J.; Laskin, A., Time-resolved molecular
580 characterization of limonene/ozone aerosol using high-resolution electrospray ionization mass
581 spectrometry. *Physical Chemistry Chemical Physics* **2009**, *11*, (36), 7931-7942.
- 582 46. Chen, X.; Hopke, P. K.; Carter, W. P. L., Secondary Organic Aerosol from Ozonolysis of
583 Biogenic Volatile Organic Compounds: Chamber Studies of Particle and Reactive Oxygen Species
584 Formation. *Environmental science & technology* **2011**, *45*, (1), 276-282.

- 585 47. Grigorev, A. E.; Makarov, I. E.; Pikaev, A. K., FORMATION OF CL₂- IN THE BULK SOLUTION
586 DURING THE RADIOLYSIS OF CONCENTRATED AQUEOUS-SOLUTIONS OF CHLORIDES. *High Energy*
587 *Chemistry* **1987**, *21*, (2), 99-102.
- 588 48. Deegan, R. D.; Bakajin, O.; Dupont, T. F.; Huber, G.; Nagel, S. R.; Witten, T. A., Capillary flow
589 as the cause of ring stains from dried liquid drops. *Nature* **1997**, *389*, (6653), 827-829.
- 590 49. Romonosky, D. E.; Ali, N. N.; Saiduddin, M. N.; Wu, M.; Lee, H. J.; Aiona, P. K.; Nizkorodov, S.
591 A., Effective absorption cross sections and photolysis rates of anthropogenic and biogenic secondary
592 organic aerosols. *Atmos. Environ.* **2016**, *130*, 172-179.
- 593 50. de Gouw, J. A.; Goldan, P. D.; Warneke, C.; Kuster, W. C.; Roberts, J. M.; Marchewka, M.;
594 Bertman, S. B.; Pszenny, A. A. P.; Keene, W. C., Validation of proton transfer reaction-mass
595 spectrometry (PTR-MS) measurements of gas-phase organic compounds in the atmosphere during
596 the New England Air Quality Study (NEAQS) in 2002. *J. Geophys. Res.-Atmos.* **2003**, *108*, (D21), 18.
- 597 51. de Gouw, J.; Warneke, C., Measurements of volatile organic compounds in the earths
598 atmosphere using proton-transfer-reaction mass spectrometry. *Mass Spectrom. Rev.* **2007**, *26*, (2),
599 223-257.
- 600 52. Baasandorj, M.; Millet, D. B.; Hu, L.; Mitroo, D.; Williams, B. J., Measuring acetic and formic
601 acid by proton-transfer-reaction mass spectrometry: sensitivity, humidity dependence, and
602 quantifying interferences. *Atmospheric Measurement Techniques* **2015**, *8*, (3), 1303-1321.
- 603 53. Renbaum-Wolff, L.; Grayson, J. W.; Bateman, A. P.; Kuwata, M.; Sellier, M.; Murray, B. J.;
604 Shilling, J. E.; Martin, S. T.; Bertram, A. K., Viscosity of alpha-pinene secondary organic material and
605 implications for particle growth and reactivity. *Proc. Natl. Acad. Sci. U. S. A.* **2013**, *110*, (20), 8014-
606 8019.
- 607 54. Warneke, C.; van der Veen, C.; Luxembourg, S.; de Gouw, J. A.; Kok, A., Measurements of
608 benzene and toluene in ambient air using proton-transfer-reaction mass spectrometry: calibration,
609 humidity dependence, and field intercomparison. *Int. J. Mass. Spectr.* **2001**, *207*, (3), 167-182.
- 610 55. Tani, A.; Hayward, S.; Hansel, A.; Hewitt, C. N., Effect of water vapour pressure on
611 monoterpene measurements using proton transfer reaction-mass spectrometry (PTR-MS).
612 *International Journal of Mass Spectrometry* **2004**, *239*, (2-3), 161-169.
- 613 56. Vlasenko, A.; Macdonald, A. M.; Sjostedt, S. J.; Abbatt, J. P. D., Formaldehyde measurements
614 by Proton transfer reaction - Mass Spectrometry (PTR-MS): correction for humidity effects.
615 *Atmospheric Measurement Techniques* **2010**, *3*, (4), 1055-1062.
- 616 57. Virkkula, A.; Van Dingenen, R.; Raes, F.; Hjorth, J., Hygroscopic properties of aerosol formed
617 by oxidation of limonene, alpha-pinene, and beta-pinene. *J. Geophys. Res.-Atmos.* **1999**, *104*, (D3),
618 3569-3579.
- 619 58. Battino, R.; Rettich, T. R.; Tominaga, T., The Solubility of Oxygen and Ozone in Liquids. *J.*
620 *Phys. Chem. Ref. Data* **1983**, *12*, (2), 163-178.
- 621 59. Kostenidou, E.; Pathak, R. K.; Pandis, S. N., An algorithm for the calculation of secondary
622 organic aerosol density combining AMS and SMPS data. *Aerosol Science and Technology* **2007**, *41*,
623 (11), 1002-1010.
- 624 60. Lienhard, D. M.; Huisman, A. J.; Krieger, U. K.; Rudich, Y.; Marcolli, C.; Luo, B. P.; Bones, D. L.;
625 Reid, J. P.; Lambe, A. T.; Canagaratna, M. R.; Davidovits, P.; Onasch, T. B.; Worsnop, D. R.; Steimer, S.
626 S.; Koop, T.; Peter, T., Viscous organic aerosol particles in the upper troposphere: diffusivity-
627 controlled water uptake and ice nucleation? *Atmos. Chem. Phys.* **2015**, *15*, (23), 13599-13613.
- 628 61. Price, H. C.; Murray, B. J.; Mattsson, J.; O'Sullivan, D.; Wilson, T. W.; Baustian, K. J.; Benning,
629 L. G., Quantifying water diffusion in high-viscosity and glassy aqueous solutions using a Raman
630 isotope tracer method. *Atmos. Chem. Phys.* **2014**, *14*, (8), 3817-3830.
- 631 62. Price, H. C.; Mattsson, J.; Zhang, Y.; Bertram, A. K.; Davies, J. F.; Grayson, J. W.; Martin, S. T.;
632 O'Sullivan, D.; Reid, J. P.; Rickards, A. M. J.; Murray, B. J., Water diffusion in atmospherically relevant
633 alpha-pinene secondary organic material. *Chemical Science* **2015**, *6*, (8), 4876-4883.

- 634 63. Chenyakin, Y.; Ullmann, D. A.; Evoy, E.; Renbaum-Wolff, L.; Kamal, S.; Bertram, A. K.,
635 Diffusion coefficients of organic molecules in sucrose-water solutions and comparison with Stokes-
636 Einstein predictions. *Atmos. Chem. Phys.* **2017**, *17*, (3), 2423-2435.
- 637 64. Hems, R. F.; Hsieh, J. S.; Slodki, M. A.; Zhou, S.; Abbatt, J. P. D., Suppression of OH Generation
638 from the Photo-Fenton Reaction in the Presence of α -Pinene Secondary Organic Aerosol Material.
639 *Environmental Science & Technology Letters* **2017**, *4*, (10), 439-443.

640

641 TOC IMAGE (We confirm that the photo was taken by the first author of this publication)



642

643